Electronic properties of B and Al doped *graphane*: A hybrid density functional study

R. E. Mapasha[a,*], E. Igumbor[a], N.F. Andriambelaza[a], N. Chetty[a,b]

[a] *Department of Physics, University of Pretoria, Hatfield campus, Pretoria 0002, RSA*
[b] *National Institute for Theoretical Physics, Johannesburg, 2000, RSA*

Abstract

Using a hybrid density functional theory approach parametrized by Heyd, Scuseria and Ernzerhof (HSE06 hybrid functional), we study the energetics, structural and electronic properties of a *graphane* monolayer substitutionally doped with the B (B_{CH}) and Al (Al_{CH}) atoms. The B_{CH} defect can be integrated within a *graphane* monolayer at a relative low formation energy, without major structural distortions and symmetry breaking. The Al_{CH} defect relaxes outward of the monolayer and breaks the symmetry. The density of states plots indicate that B_{CH} doped *graphane* monolayer is a wide band gap semiconductor, whereas the Al_{CH} defect introduces the spin dependent mid gap states at the vicinity of the Fermi level, revealing a metallic character with the pronounced magnetic features. We further examine the response of the Al dependent spin states on the multiple charge states doping. We find that the defect formation energy, structural and electronic properties can be altered via charge state modulation. The +1 charge doping opens an energy band gap of 1.75 eV. This value corresponds to the wavelength in the

*Corresponding author
Email address: edwin.mapasha@up.ac.za (R. E. Mapasha)

visible spectrum, suggesting an ideal material for solar cell absorbers. Our study fine tunes the *graphane* band gap through the foreign atom doping as well as via defect charge state modulation.

Keywords: *Graphane*, Defect, Electronic structure

1. Introduction

Recently, two-dimensional (2D) material systems such as the graphene [1], *graphane* [2], hexagonal boron nitride [3] and transition metal dichalcognides [4] monolayers have attracted great research interests owing to their peculiar electronic properties. A relatively high charge carrier mobility indicated by the linear dispersion-like at the Dirac-point in the electronic spectrum of a graphene monolayer exposes its semi-metallic character [1, 5, 6, 7, 8]. The absence of the band gap is a setback for the direct integration of the graphene thin films into the electronic devices. To make graphene electronically viable, alteration of its electronic structure and prediction of other new graphene-related 2D material systems have become intensive topics. The *graphane*, hexagonal boron nitride and transition metal dichalcognides monolayers are amongst those predicted, and are wide band gap semiconductors [2, 3, 9, 10, 11, 12].

The *graphane* thin films were experimentally synthesized by *Elias et al.* [13] under hydrogen plasma surrounding as free standing materials. It was reported that the experimental characterization of the *graphane* samples reveals that they are thermodynamically stable at room temperature and possess insulating features, although the magnitude of the band gap was not quantified [13]. Based on this and also considering its relatively thin

membrane [14], *graphane* may be suitable for current nanoelectronic technology. Depending on the type of exchange-correlation functional employed, the density functional theory (DFT) calculations predict *graphane* to have the direct band gap of 3.40 eV [15] using a Perdew, Burke and Ernzerhof generalized gradient approximation (PBE-GGA) [16] functional and 4.38 eV [17] for a Heyd, Scuseria and Ernzerhof (HSE06) [18] hybrid functional. The underestimation of the band gap by a PBE-GGA functional is due to its self-interaction leading to underbinding of localized states. A HSE06 functional reduces this by mixing a 25% fraction of Hartree-Fock exchange with 95% fraction of a PBE-GGA functional for the short-range exchange potential part [18]. A HSE06 functional has been known to accurately predict the band gap of semiconductors [18] and the defects charge state transition levels [19].

Modulating the electronic properties of the nanostructure materials is essential for the technological device operations. Since *graphane* belongs to the class of the 2D systems which have low dimensionality [14], it can be modified at an atomic level without difficulty. In a *graphane* monolayer, every C atom is in the sp^3 hybridization with its nearest neighbour three C atoms and one H atom. Ideally, *graphane* is fully saturated, and it is not expected to possess any valuable magnetic features. To alter the electronic structure of *graphane*, vacancies and dopants are the possible options. The hydrogen (H) vacancy is a simple defect one can create [20, 21]. Pujari *et al.* [22] reported that the C-H vacancy pair is also a possible defect, and can form with a lower energy than the H vacancy.

The B and N atom substitutions create the p-type and n-type doping

in a *graphane* monolayer respectively, and also causes the semiconductor to metallic transition [23, 24]. It was suggested that a *graphane* monolayer can be a useful base for creating new nanotechnological devices. These recent DFT studies focused on replacing the C atom in a *graphane* monolayer i.e. B_C, N_C, Al_C and P_C [23, 24]. The information on replacing a C-H pair with foreign atoms has not been reported before, and is worth to be investigated. The substitution of a C-H pair with solid atoms such as B and Al although has not yet reported can be achievable experimentally through ion implantation. Considering the fact that creation of the C-H pair leaves its three nearest neighbour C atoms dangling, each with an unpaired electron, therefore an introduction of the B atom having three excited valence electrons at this vacancy site should cause saturation through electron pairing. Thus, influence of the B_{CH} defect should be structural instead of chemical in this case.

In this work, we study the thermodynamic stability, structural and electronic properties of B_{CH} and Al_{CH} defects in a *graphane* monolayer using a HSE06 hybrid DFT approach. Considering the inability of the standard DFT functionals to accurately predict the band gap, a HSE06 functional is employed. Our results reveal that the B_{CH} doped *graphane* monolayer is a wide band gap semiconductor, whereas the Al_{CH} defect induces spin dependent states crossing the Fermi level, showing a metallic character. We further examine the influence of the intrinsic charge doping on the Al induced spin dependent states. This study fine tunes the band gap of *graphane* through the foreign atom doping as well as via changing the charge state of the defect.

2. Computational details

Our first-principles electronic structure calculations are performed using the DFT approach implemented within the Vienna *ab initio* simulation package (VASP) code [25]. These calculations are carried out with the projector augmented wave (PAW) pseudopotential plane-wave method [26]. For the exchange-correlation interactions, a HSE06 functional is employed [18]. For energetics comparison, a GGA-PBE functional is also employed. For the start of each calculation, the electronic spin is tuned on. The energy cut-off was set to 500 eV for expanding the plane wavefunctions. The structural geometries are allowed to relax until each atomic force is less than 0.01 eVÅ^{-1} and the total energies are converged to 10^{-7} eV.

The defect formation energy is defined as;

$$E_{form}(X) = E_X - E_{graphane} + \mu_C + \mu_H - \mu_X + q[E_F + E_V] + \Delta^q_{MP}. \quad (1)$$

The first two terms E_X and $E_{graphane}$ are the total energies of B or Al doped *graphane* and pristine *graphane* respectively. The μ_C and μ_H terms are the chemical potentials of the host C atom (obtained as the total energy per C atom from the unit cell of graphene monolayer) and H atom (obtained as the total energy per H atom from the hydrogen molecule), whereas the μ_X term is the chemical potential of the B defect (obtained as the total energy per B atom from α rhombohedral B structure) or Al defect (obtained as the total energy per Al atom from the Al face centered cube structure) respectively. E_F is the Fermi level position referenced to the valence band maximum (VBM) in the pristine *graphane* structure, whereas E_V is the energy corresponding to the VBM of the defect. The Makov-Payne [27] correction term

(Δ^{q}_{MP}) is added to Eqn.1 to eliminate the energy errors that might arise due to the effects of the spurious electrostatic interactions of the doped charge with its periodic image. The complete expression of Δ^{q}_{MP} can be found in reference [27].

The following supercell convergence tests are carried out to reduce the fictitious defect-defect interactions from the periodic images along the *xy* plane. The B and Al atoms individually substituting the C-H pair in the 4×4, 5×5, 6×6, 7×7 and 8×8 *graphane* supercell sizes are considered on the formation energy analyses employing a PBE-GGA functional. The formation energy for the B defect obtained using Eqn.1 is 0.48 eV (4×4), 0.89 eV (5×5), 0.94 eV (6×6), 0.97 eV (7×7) and 0.99 eV (8×8). The formation energy difference ΔE between the next and previous supercell is 0.42 eV, 0.04 eV, 0.03 eV and 0.02 eV. This trend agrees very well with that of Leenaerts *et al.* [28] for B atom replacing C atom in a fluorographene monolayer. The formation energy for the Al defect is 2.09 eV (4×4), 3.19 eV (5×5), 3.49 eV (6×6), 3.50 eV (7×7) and 3.51 eV (8×8) with the ΔE of 1.10 eV, 0.30 eV, 0.01 eV, 0.01 eV. For both defects, ΔE indicates that the 6×6 supercell size is sufficient to correctly describe the properties of the defect. For this supercell size, the 2×2×1 k-point meshes generated using the Monkhorst-Pack scheme [29] are used for structural relaxation, and increased to 10×10×1 for the density of states (DOS) calculations. The converged 20 Å spacing was set to isolate the *graphane* layers along the *z* axis.

Graphane can appear in different H isomers such as boat, chair, armchair etc. An overview of all the *graphane* isomers are found in the review paper of Sahin *et al.* [14]. Amongst all the isomers mentioned, the chair isomer is the

most thermodynamically stable structure [14], and it was accomplished spontaneously during the graphene hydrogen plasma exposure [13]. Based on this, all our calculations are performed using the *graphane* chair isomer depicted in Fig.1(a). The ground state properties of the chair-like *graphane* obtained using the HSE06 and GGA-PBE functionals are presented in Table 1. Both the functionals predict nearly the same structural properties of *graphane*, although a HSE06 functional shows slight underestimation of about 1 mÅ. This trend is supported by the previous studies [17, 30]. As expected, a HSE06 functional predicts larger band gap values of the pristine *graphane* structure than a GGA-PBE functional. Since there is no experimental band gap value for *graphane*, Karlicky*et al.* [30] calculated the HSE06 band gap of fluorographene and found that it agrees very well with the available experimental band gap value. Since the *graphane* and fluorographene monolayers have the same bonding network and structural arrangement, our HSE06 band gap value should agree with the future experimental data. Based on these results, our conclusions are made relative to a HSE06 functional in the subsequent calculations of B_{CH} and Al_{CH} defects in a *graphane* monolayer.

3. Results and discussion

As mentioned earlier, we study the properties of the B and Al atoms substituting the C-H pair in a 6×6 supercell *graphane* monolayer, named as B_{CH} and Al_{CH} defects respectively, as shown in Fig.1. To examine the influence of the B and Al substitutional defects on the *graphane* structure, the selected distances between the nearest neighbour carbon atoms (L_1) and the distances between the defect and its nearest neighbour C atoms denoted as

Table 1: The calculated equilibrium lattice constant a_0 (in Å), the distance between the two nearest neighbour carbon atoms d_{C-C} (in Å), the carbon buckling height Δ_{h_C} (in Å), the distance between the carbon and nearest neighbour hydrogen atoms d_{C-H} (in Å) and energy band gap E_{gap} (in eV).

	Methods	a_0	d_{C-C}	Δ_{h_C}	d_{C-H}	E_{gap}
This work	HSE06	2.52	1.53	0.44	1.10	4.51
	GGA-PBE	2.54	1.54	0.46	1.11	3.38
Other work	HSE06	2.52[a]	1.53[a]		1.10[a]	4.60[a]
	HSE06	2.52[b]	1.53[b]			4.38[b]
	GGA-PBE	2.54[c]	1.54[c]		1.12[c]	3.50[c]
	GGA-PBE	2.52[d]	1.52[d]		1.10[d]	3.50[d]
	GGA-PBE	2.54[e]		0.46[e]		

[a]Ref[30]. [b]Ref [17]. [c]Ref [14, 28]. [d]Ref [2]. [e]Ref [31].

L_2, L_3 and L_4 as shown in Fig.1 are measured. We compare our energetics and electronic properties of B_{CH} and Al_{CH} defects with those of B atom and Al atom substituting the C only, named as B_C defect and Al_C defect reported in reference [24]. For comparison sake, we also calculate the formation energies for B_{CH} and Al_{CH} defects using a GGA-PBE functional to compare with those of B_C and Al_C defects from reference [24] obtained using the same functional.

3.1. The B_{CH} defect

Firstly, we investigate the stability of the B_{CH} defect from the formation energy (E_{form}) analysis obtained using Eqn.1. The E_{form} of B_{CH} defect is 1.05 eV (HSE06), comparable to a GGA-PBE value of 0.94 eV. In principle, the positive E_{form} means that the structure is thermodynamically unstable

(endothermic reaction), may not form spontaneously during the growth, but can be accomplished experimentally via high energy pathways such as ion beam deposition. Wang *et al.* [24] reported the E_{form} of 4.51 eV for B_C using a GGA-PBE exchange-correlation functional. Interestingly, the B_{CH} defect E_{form} value is 3.52 eV less than that of B substituting the C host atom (B_C), calculated using the same functional. This suggests that the B_{CH} defect can be accomplished experimentally at a relatively low energy compared to the synthesis of B_C defect.

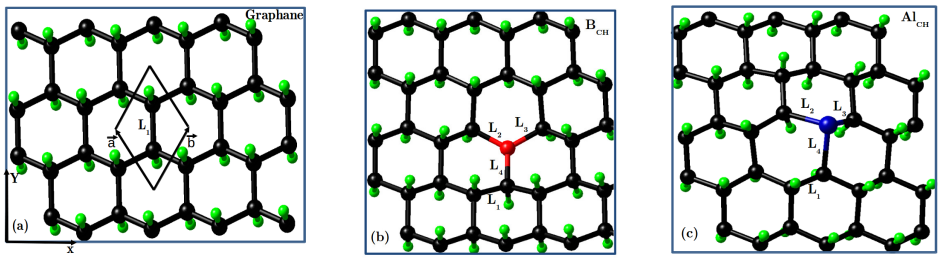

Figure 1: (a) The relaxed geometry of a pristine *graphane* chair isomer monolayer. The parallelogram shape indicates the unit cell of a *graphane* monolayer having the two C atoms and two H atoms, where $\vec{a}$ and $\vec{b}$ are the lattice vectors which their magnitudes are equal to a_0 presented in Table 1. The relaxed geometries of (b) B doped *graphane* (B_{CH}) and (c) Al doped *graphane* (Al_{CH}) defects. The C and H host atoms are indicated by the black and light green spheres, whereas the B and Al defects are indicated by the red and blue spheres respectively. The C-C bondlength (d_{C-C}) is represented by the variable L_1, whereas the three C-B/Al bondlengths are represented by the variables L_2, L_3 and L_4.

In comparison, our calculated C-C bond distances (L_1) in a pristine *graphane* monolayer are uniformly at 1.53 Å, when calculated using a HSE06 functional. The fully relaxed three C-B bond distances are $L_2 = L_3 = L_4 =$ 1.53 Å(see the fully relaxed Fig.1(b)). Comparing the magnitudes of the C-C and C-B bond distances, it is evident that the B_{CH} defect does not impose

significant structural distortion in a *graphane* monolayer. The B buckling height Δ_{h_B} is 0.44 Å equal to that of C in a *graphane* monolayer shown in Table 1. Since L_2, L_3 and L_4 distances are identical, and equal to the uniform C-C distances (L_1), we conclude that the B atom can easily integrate in a *graphane* supercell without breaking the hexagonal symmetry.

To examine the nature of binding in the B-C bond, we calculate the amount of charge transfer by performing Bader charge density analyses [32]. The B atom defect has a charge transfer of +1.90 e, its three nearest neighbour bonded C atoms possess -0.75 e each and their H atoms counterparts each has +0.1 e. The positive charge transfer in the B and H atoms indicates that there is a significant charge flow from the B atom to the C host atoms. The identical amount of charge transfer of -0.75 e accepted by each nearest neighbour C atom emphasizes the fact that the hexagonal symmetry remains.

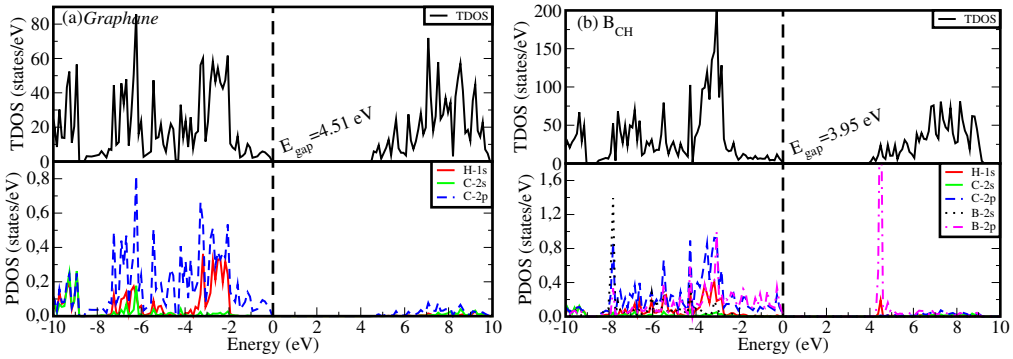

Figure 2: (a) The total density of states (TDOS) and partial density of states (PDOS) of the H and C atoms in a pristine *graphane* monolayer. (b) The TDOS and PDOS of the H, C and B atoms in the B_{CH} defect. The Fermi level is set to 0 eV and marked by the dashed line.

To gain insights into the electronic structure of B_{CH} defect in a *graphane* monolayer, the DOS are plotted as shown in Fig. 2. Fig. 2(a) depicts the DOS of a pristine *graphane* structure, the TDOS are shown on the top panel and the PDOS on the bottom panel. The TDOS plot reveals that *graphane* is a wide band gap semiconductor with the value of 4.51 eV (HSE06) between the VBM and CBM. This band gap value compares very well with the literature values of 4.38 eV [17] and 4.50 eV [30] obtained using the same functional. Fig. 2(b) depicts the DOS of B_{CH} defect in a *graphane* monolayer. We find that the B_{CH} defect retains the wide band gap semiconducting behaviour of a *graphane* monolayer host, although with a reduced band gap value of 3.95 eV as shown in Fig. 2(b). The bottom panel in Fig. 2(b) shows that this reduction is mainly caused by contribution of the B p orbital states with a pronounced peak and H s orbital states occupying 0.56 eV of energy below the conduction band minimum (CBM). This is in contrast with B_C defect which exhibits a metallic character [24].

The B_{CH} defect in a *graphane* monolayer has no total magnetic moment (TMM = 0.00 μ_B per supercell). We calculate the magnetization energy (ΔE_{mag}) of B_{CH} defect as the energy difference between the total energy of the spin-polarized system (spin imposed in the B_{CH} defect) and that of the non-spin-polarized system (spin not imposed in the B_{CH} defect). The magnitude of the magnetization energy is the energy gained when the electronic spins are imposed in the system and favours magnetism. In the B_{CH} defect, the $\Delta E_{mag} = 0.00$ eV, revealing that the system is non-magnetic.

3.2. The Al_{CH} defect

We investigate stability of the Al_{CH} defect from the E_{form} analysis obtained using Eqn.1. The E_{form} of Al_{CH} defect is 3.55 eV for HSE06 and 3.49 eV for GGA-PBE. Wang *et al.* [24] reported the GGA-PBE formation energy of 9.98 eV for Al_C. This suggests that under equilibrium conditions, the Al_{CH} defect is more likely to form than the Al_C defect, although not spontaneously but via high energy pathways.

Fig.1(c) shows the effects of Al_{CH} defect on the geometrical structure of a *graphane* monolayer. After structural relaxation, the Al defect buckled out of the *graphane* structure (along the z-axis of the cell) shown in Fig.1(c). The Al defect relaxes outward of a *graphane* monolayer to a buckling height ($\Delta_{h_{Al}}$) of 1.45 Å measured from the topmost carbon atoms (its nearest neighbour C atoms). This value is significantly larger than that of Δ_{h_c} presented in Table 1. The three inequivalent C-Al bond distances L_2, L_3 and L_4 (shown in Fig.1(c)) are 2.03 Å, 2.03 Å and 1.89 Å respectively, larger than the L_1 value of 1.53 Å in a *graphane* monolayer. The inequivalent bond distances L_2, L_3 and L_4 reveal that the Al defect breaks the symmetry of a *graphane* structure. Similar to the B_{CH} defect, we investigate the nature of binding in the C-Al bond by calculating the amount of charge transfer. We find that Al defect gives +1.45 e charge, and the two C atoms that form L_2 and L_3 each receives -0.44 e charge. The C atom which forms short bond distance L_4 receives slightly larger amount of charge of -0.53 e.

Fig. 3(a) depicts the DOS of Al_{CH} in a *graphane* monolayer. We see that the Al_{CH} defect introduces the majority high spin states crossing the Fermi level within the band gap, revealing a metallic character. The bottom panel

in Fig. 3(a) shows that the introduced high spin defect states are mainly contributed by Al-3s and Al-3p orbital states. This is in agreement with Al_C defect in a *graphane* monolayer, although the metallic character arises from the minority spin channel [24]. The spin splitting shown at the vicinity of the Fermi level in Fig. 3(a) for Al_{CH} defect in a *graphane* monolayer yields a total magnetic moment (TMM) of 2.00 μ_B double as compared to that of Al_C reported in reference [24]. For the Al_{CH} defect, ΔE_{mag} is 253 meV revealing that the system tend to be magnetic. This value is far more than the room temperature thermal energy of about 25 meV indicating that the Al induced magnetism in the *graphane* monolayer is stable.

We now examine the effects of charge doping on the thermodynamic stability, structural and electronic properties of the Al_{CH} defect in the *graphane* structure. The main objective is to examine the response of Al induced high spin states on the charge doping. Firstly, we consider the following charge states for the Al_{CH} defect; -3, -2, -1, 0, +1, +2 and +3 to cover all the valence electrons in Al, denoted as $Al^{-3}{}_{CH}$, $Al^{-2}{}_{CH}$, $Al^{-1}{}_{CH}$, $Al^{0}{}_{CH}$, $Al^{+1}{}_{CH}$, $Al^{+2}{}_{CH}$ and $Al^{+3}{}_{CH}$. Our calculated E_{form} of the Al_{CH} defect in these different charge states are constrained to vary within the band gap of a pristine *graphane* monolayer (from 0 eV (VBM) to 4.51 eV (CBM)) as a function of the Fermi level position shown in Fig. 3(b). This is to examine the thermodynamic stability of the considered charge states within the band gap.

Fig. 3(b) shows that the following charge states; -3, 0, +2 and +3 are not thermodynamically stable within the band gap. At the p-type region, mostly at the VBM (E_F = 0 eV), the +1 charge state ($Al^{+1}{}_{CH}$) is most

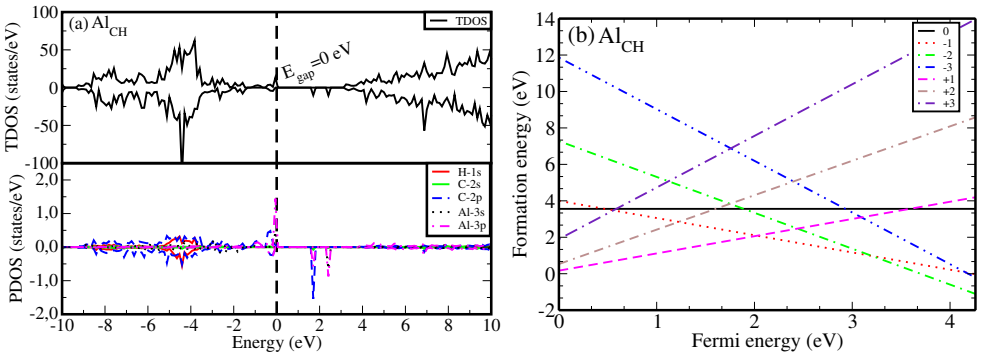

Figure 3: (a) The DOS of the Al_{CH} defect in a *graphane* monolayer. Top and bottom panels present the TDOS and PDOS respectively. (b)The formation energies of Al_{CH} in the charge states -3, -2, -1, 0, +1, +2 and +3 as a function of the Fermi level. The slope of each graph corresponds to the charge state as defined in Eqn.1.

stable with the formation energy of 0.13 eV far less than that of $Al^0{}_{CH}$. The +1 charge state continues to dominate almost the bottom half of the band gap up to E_F = 1.92 eV. Moreover, this suggests that at the p-type region, the Al_{CH} defect may act as a single donor providing one electron, and its concentration is dominant. Fig. 3(b) also shows that the -1 and -2 charge states dominate the top half of the band gap (n-type region). At the CBM (E_F = 4.51 eV), the formation energy of the $Al^{-2}{}_{CH}$ defect is -1.50 eV revealing the thermodynamic stable acceptor defect. In summary, our results suggest that Al_{CH} defect acts as a donor as well as acceptor depending on the type of charge state and position of E_F.

Table 2 summarizes the effects of charge doping on the Al induced structural properties. The -1 charge doping reduces the bond distances L_2 and L_3 by 0.11 Å, while slightly increasing L_4 by 0.02 Å after structural optimization. The noted structural rearrangement leads to equal bondlengths L_2 =

Table 2: The dependence of the Al induced structural properties on the multiple stable stable charge states (-2, -1, 0, +1 and +2). The optimized bondlengths (Å) L_2, L_3 and L_4 are the distances between Al and its nearest neighbour C atoms. The $\Delta_{h_{Al}}$ (Å) is the buckling height of Al defect measured from its nearest neighbour topmost C atoms in the *graphane* monolayer. The dependence of the Al induced total magnetic moment TMM (μ_B) on the multiple stable charge states.

Properties	-2	-1	0	+1	+2
L_2	1.92	1.92	2.03	2.19	2.19
L_3	1.92	1.92	2.03	2.19	2.19
L_4	1.92	1.92	1.89	1.92	1.92
$\Delta_{h_{Al}}$	0.90	0.90	1.45	1.62	1.62
TMM	2.02	1.05	2.00	1.09	0.47

$L_3 = L_4 = 1.92$ Å in Al_{CH} defect. This suggests that the -1 charge doping regains the initial symmetry of *graphane*, although the C-Al distances are still more than C-C distance by 0.4 Å. Further more, this structural rearrangement reduces $\Delta_{h_{Al}}$ from 1.45 Å to 0.90 Å. The addition of -2 charge state does not impose any further structural improvement on -1 charge state. When a hole (+1 charge) is doped into Al_{CH} defect, different scenario is noted. The bondlengths L_2, L_3 and L_4 elongate by 0.16 Å, 0.16 Å and 0.03 Å respectively. Consequently, the structural symmetry remains broken after structural optimization. This structural rearrangement elongates $\Delta_{h_{Al}}$ by 0.17 Å. The extremely large value of the bondlength in most cases leads to ionic bonding character instead of covalent bond.

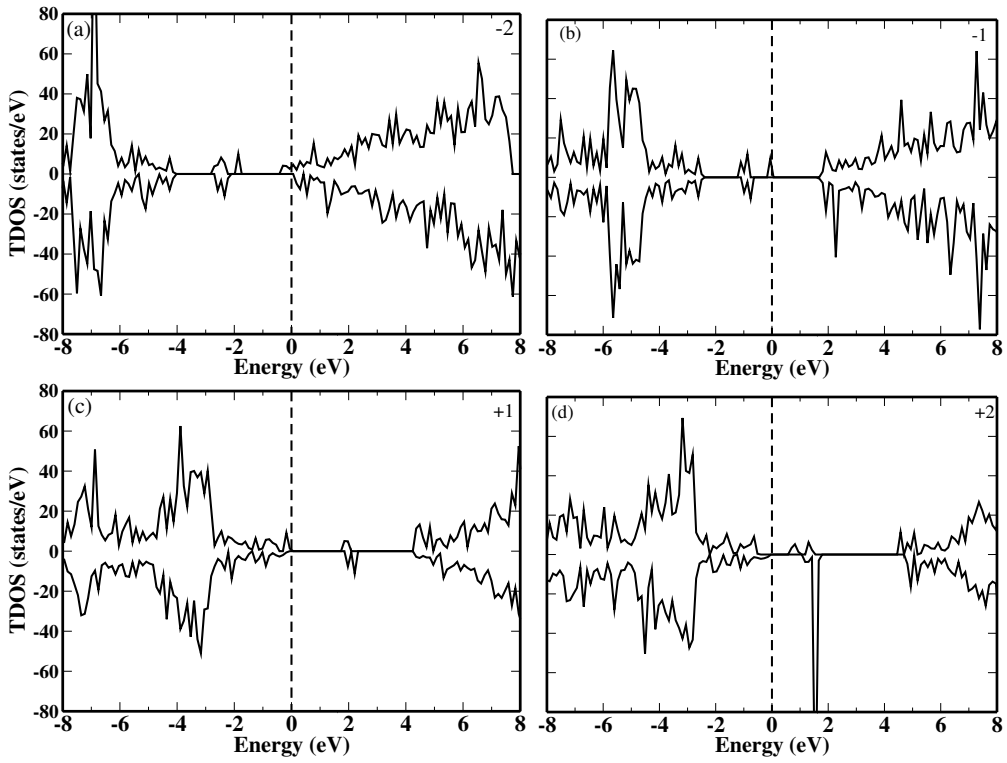

Figure 4: The TDOS for the stable charge states -2, -1, +1 and +2; i.e. (a) $Al^{-2}{}_{CH}$, (b) $Al^{-1}{}_{CH}$, (c) $Al^{+1}{}_{CH}$ and (d) $Al^{+2}{}_{CH}$. The Fermi level is marked by the dashed line.

Lastly, we examine the role of charge doping on the electronic properties of Al_{CH} defect by analyzing the DOS shown in Fig. 4. Comparing the DOS for $Al^0{}_{CH}$ shown in Fig. 3(a) and the DOS for $Al^{-1}{}_{CH}$ shown in Fig. 4(b), it is noted that the -1 charge doping shifts both the E_F and Al induced high spin up states by 1.05 eV, and positions them at 2.36 eV away from the VBM. This shifts reduces the TMM to 1.05 μ_B per supercell shown in Table 2. Interestingly, the $Al^{-1}{}_{CH}$ defect exhibits an extrinsic half-metallic character which is another domain for spin based electronic devices. The -2 charge doping separates the Al dependent spin states from the E_F, and place the E_F into the CBM (see Fig. 4). Revealing the excess of electrons (n-type) in the $Al^{-2}{}_{CH}$ system. This system regains the TMM of 2.02 μ_B.

Comparing the DOS for $Al^0{}_{CH}$ shown in Fig. 3(a) and Dos for $Al^{+1}{}_{CH}$ shown in Fig. 4(c), it is noted that the +1 charge doping shifts the E_F as well as the Al dependent spin states towards the VBM, although not in equal magnitude. Thus, the difference in shifting opens the band gap of 1.75 eV. The obtained band gap value corresponds to the wavelength in the visible spectrum, suggesting that $Al^{+1}{}_{CH}$ can be an ideal material for solar cell absorbers considering the high charge carrier mobility in this type of systems. This system ($Al^{+1}{}_{CH}$) possesses the total magnetic moment of 1.09 μ_B per supercell which is a reduction compared to that of $Al^0{}_{CH}$ of 2.00 μ_B. The +2 charge doping ($Al^{+2}{}_{CH}$) possesses a semiconducting features with the narrow band gap of 0.50 eV as shown in Fig. 4(d) and further reduces TMM to 0.47 μ_B as shown in Table 2. The noted variation in the magnetic moment indicates that the charge doping can also be an effective way of controlling the Al induced magnetism in the *graphane* monolayer.

4. Conclusions

In summary, we study the electronic structure of B doped *graphane* (B_{CH}) as well as Al doped *graphane* (Al_{CH}) using a HSE06 hybrid functional within the framework of the DFT approach. We find that the B_{CH} defect can form at a relative low formation energy compared to the B_C defect, *albeit* endothermically. The B_{CH} defect can easily be integrated within the *graphane* monolayer without causing significant structural distortion and breaking the symmetry. The PDOS analysis reveals that B_{CH} defect introduces a pronounced sharp peak arising from the B $2p$ orbital state below the CBM, leading to the reduction of the band gap by 0.56 eV.

The Al_{CH} defect forms at a relative low formation energy compared to Al_C defect in a *graphane* monolayer, although endothermically. The Al_{CH} defect relaxes outward of the monolayer to a buckling height of 1.45 Å, and also breaks the symmetry of the system. The Al_{CH} defect introduces a high spin mid-gap states at the Fermi level arising from the Al-3s and Al-3p orbital states, exhibiting a metallic character. We further examine the response of the Al dependent spin states on the multiple charge states doping. We find that the defect formation energy, structural and electronic properties can be altered via charge state modulation. The +1 charge doping is most thermodynamically stable through out the bottom half of a *graphane* band gap, and opens the band gap of a Al_{CH} system of 1.75 eV by shifting the Al dependent spin states towards the VBM. This value corresponds to the wavelength in the visible spectrum, suggesting an ideal material for solar cell absorbers. Our study adequately fine tunes the *graphane* band gap through the foreign atom doping as well as via defect charge state modulation. The

Al_{CH} defect induces the stable magnetism with the pronounced magnetic moment and relatively high magnetization energy. The charge doping can be a prominent way of controlling the Al induced magnetism in the *graphane* monolayer.

Acknowledgment

This work was financially supported by the University of Pretoria and National Research Foundation. The authors would like to thank the University of Pretoria for computational resources. NC thanks the National Institute for Theoretical Physics for financial support.

References

[1] K. S. Novoselov, A. K. Geim, S. V. Morozov, D. Jiang, Y. Zhang, S. V. Dubonos, I. V. Grigorieva, and A. A. Firsov, *Science* **306**, 666 (2004).

[2] J. O. Sofo, A. S. Chaudhari, and G. D. Barber, *Phys. Rev. B* **75**, 153401 (2007).

[3] K. Watanabe, T. Taniguchi, and H. Kanda, *Nat. Mater.* **3**, 404 (2004).

[4] A. D. Yoffe, *Chem. Soc. Rev.* **5**, 51 (1976).

[5] A. K. Geim and K. S. Novoselov, *Nature Mater.* **6**, 183 (2007).

[6] P. R. Wallace, *Phys. Rev.* **71**, 622 (1947).

[7] K. S. Novoselov, A. K. Geim, S. V. Morozov, D. Jiang, Y. Zhang, M. I. Katsnelson, S. V. Dubonos, I. V. Grigorieva, and A. A. Firsov, *Nature (London)* **438**, 197 (2005).

[8] K. S. Novoselov, Z. Jiang, Y. Zhang, S. V. Morozov, H. L. Stormer, U. Zeitler, J. C. Maan, G. S. Boebinger, P. Kim, and A. K. Geim, *Science* **315**, 1379 (2007).

[9] L. Song, L. Ci, H. Lu, P. B. Sorokin, C. Jin, J. Ni, A. G. Kvashnin, D. G. Kvashnin, J. Lou, B. I.Yakobson, and P. M. Ajayan, *Nano Lett.* **10**, 3209 (2010).

[10] D. Golberg, Y. Bando, Y. Huang, T. Terao, M. Mitome, C. Tang, and C. Zhi, *ACS Nano.* **4** 2979-2993 (2010).

[11] J. A. Wilson and A. D. Yoffe, *Adv. Phys.* **18**, 193 (1969).

[12] R. H. Friend and A. D. Yoffe, *Adv. Phys.* **36**, 1 (1987).

[13] D. C. Elias, R. R. Nair, T. M. G. Mohiuddin, S. V. Morozov, P. Blake, M. P. Halsall. A. C. Ferrari, D. W Boukhvalov, M. I. Katsnelson, A. K. Geim, and K. S. Novoselov, *Science* **323**, 610 (2009).

[14] H. Sahin, O. Leenaerts, S. K. Singh, and F.M. Peeters, *WIREs: Comp. Mol. Sci.* **5**, 255 (2015).

[15] H. Sahin, C. Ataca, and S. Ciraci, *Phys. Rev. B* **81**, 205417 (2010).

[16] J. P. Perdew, K. Burke, and M. Ernzerhof, *Phys. Rev. Lett.* **77**, 3865 (1996).

[17] M. N. Amini, O. Leenaerts, B. Partoens, and D. Lamoen, *J. Phys. Chem. C*, **117**, 16242-16247 (2013).

[18] J. Heyd, G. E. Scuseria, and M. Ernzerhof, *J. Chem. Phys.* **118**, 8207 (2003); **124**, 219906 (2006).

[19] C. G. Van de Walle and J. Neugebauer, J. Appl. Phys. **95**, 3851 (2004).

[20] H. Sahin, C. Ataca, and S. Ciraci, *Appl. Phys. Lett.* **95**, 222510 (2009).

[21] R. E. Mapasha, M. P. Molepo, and N. Chetty, *Phys. E.* **79**, 52-58 (2016).

[22] B. S. Pujari and D.G. Kanhere, *J. Phys. Chem. C* **113**, 21063 (2009).

[23] G. Savini, A. C. Ferrari, and F. Giustino, *Phys. Rev. Lett.* **105**, 037002 (2010).

[24] Y. Wang, Y. Ding, S. Shi, and W. Tang, *Appl. Phys. Lett.* **98**, 163104 (2011).

[25] G. Kresse and J. Hafner, *Phys. Rev. B* **47**, 558 (1993).

[26] P. E. Blochl, *Phys. Rev. B* **50**, 17953 (1994).

[27] G. Makov and M. C. Payne, *Phys. Rev. B* **51**, 4014 (1995).

[28] O. Leenaerts, H. Sahin, B. Partoens, and F. M. Peeters, Phys. Rev. B **88**, 035434 (2010).

[29] H. J. Monkhorst and J. D. Pack, *Phys. Rev. B* **13**, 5188 (1976).

[30] F. Karlicky, R. Zboril and M. Otyepka, *J.Chem. Phys.* **137**, 034709 (2012).

[31] R. C. Andrew, R. E. Mapasha, and N. Chetty, J. Chem. Phys. **138**, 244709 (2013).

[32] R. F. W. Bader, Atoms in Molecules - A Quantum Theory (Oxford University Press, Oxford, 1990).